Ion-transporting capacity and aerobic respiration of larval white seabass (*Atractoscion nobilis*) may be resilient to ocean acidification conditions

Garfield T. Kwan [a,b,1], Sara G. Shen [a,1,*], Mark Drawbridge [c], David M. Checkley Jr. [a], Martin Tresguerres [a,*]

[a] *Scripps Institution of Oceanography, University of California, San Diego, La Jolla, CA, USA*
[b] *National Oceanic and Atmospheric Administration Fisheries Service, Southwest Fisheries Science Center, 8901 La Jolla Shores Drive, La Jolla, CA 92037, USA*
[c] *Hubbs-SeaWorld Research Institute, San Diego, CA, USA*

HIGHLIGHTS

- Larval white seabass was lab-exposed to elevated CO_2 levels simulating future ocean acidification (OA).
- OA exposure did not induce changes in ion-transporting capacity, aerobic respiration rate, or total length.
- Retroactive analysis of broodstock tanks revealed their parents were chronically exposed to elevated CO_2 for ≥3.5 years.
- Parental exposure may have affected the physiology of the larvae and conferred the observed resilience.

GRAPHICAL ABSTRACT
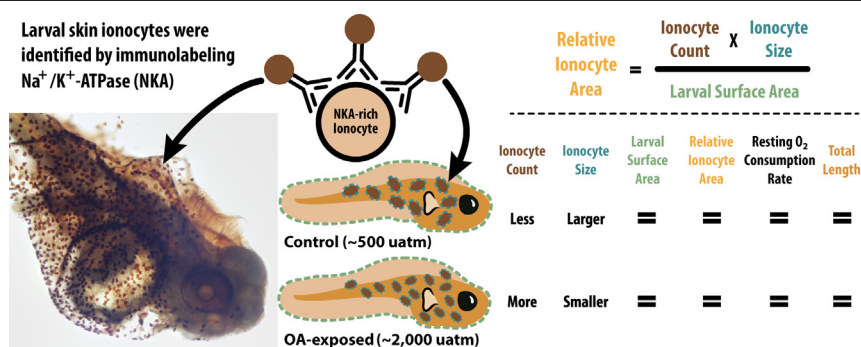
ARTICLE INFO

ABSTRACT

Ocean acidification (OA) has been proposed to increase the energetic demand for acid-base regulation at the expense of larval fish growth. Here, white seabass (*Atractoscion nobilis*) eggs and larvae were reared at control (542 ± 28 μatm) and elevated pCO_2 (1831 ± 105 μatm) until five days post-fertilization (dpf). Skin ionocytes were identified by immunodetection of the Na^+/K^+-ATPase (NKA) enzyme. Larvae exposed to elevated pCO_2 possessed significantly higher skin ionocyte number and density compared to control larvae. However, when ionocyte size was accounted for, the relative ionocyte area (a proxy for total ionoregulatory capacity) was unchanged. Similarly, there were no differences in relative NKA abundance, resting O_2 consumption rate, and total length between control and treatment larvae at 5 dpf, nor in the rate at which relative ionocyte area and total length changed between 2 and 5 dpf. Altogether, our results suggest that OA conditions projected for the next century do not significantly affect the ionoregulatory capacity or energy consumption of larval white seabass. Finally, a retroactive analysis of the water in the recirculating aquarium system that housed the broodstock revealed the parents had been exposed to average pCO_2 of ~1200 μatm for at least 3.5 years prior to this experiment. Future studies should investigate whether larval white seabass are naturally resilient to OA, or if this resilience is the result of parental chronic acclimation to OA, and/or from natural selection during spawning and fertilization in elevated pCO_2.

1. Introduction

The survival of fish during the early life stages is the serendipitous outcome of a favorable combination of oceanographic, hydrographic, climatic, biological, and trophodynamic factors (Houde, 2009). Without

* Corresponding authors.
  E-mail addresses: saragshen@gmail.com (S.G. Shen), mtresguerres@ucsd.edu (M. Tresguerres).
  [1] These authors contributed equally to this work.

the ability to swim, fish eggs, embryos and pre-flexion larvae may be advected offshore to suboptimal habitat, consumed by zooplankton and other predators, or starve before finding suitable prey (Hjort, 1926; Houde, 2009). As a result of the environment's strong control over recruitment dynamics, mortality is high and variable during the vulnerable early life stages (Beaugrand et al., 2003; Houde, 2009). Of particular concern are the impacts of climate change on larval fish survival. Under 'business-as-usual' emission scenarios, the average partial pressure of carbon dioxide (pCO$_2$) in the global surface ocean is projected to reach ~1000 µatm by the year 2100 and ~2000 µatm by the year 2300, with a corresponding decrease in pH from current levels of ~8.0 down to ~7.7 and ~7.4 respectively (Caldeira and Wickett, 2003, 2005; Meehl et al., 2007; Goodwin et al., 2018; Bindoff et al., 2019). This phenomenon, "ocean acidification" (OA), may further challenge survival during the early life stages through disturbances to acid-base homeostasis leading to physiological, energetic, or behavioral alterations (Heuer and Grosell, 2014; Esbaugh, 2017; Tresguerres and Hamilton, 2017).

Many of the reported potentially negative effects of OA on fish larvae have been attributed to their lack of gill and their Na$^+$/K$^+$-ATPase-rich (NKA) ionocytes (e.g. Ishimatsu et al., 2008; Frommel et al., 2011; Baumann et al., 2012; Pimentel et al., 2014, 2015), the primary organ for blood acid-base regulation (reviewed in Evans et al., 2005). However, this explanation dismisses the NKA-rich ionocytes found on the skin of embryonic and larval fishes (Varsamos et al., 2002; Dahlke et al., 2017, 2020; Kwan et al., 2019a; reviewed in Glover et al., 2013). As the larvae grow and their gills develop, the abundance of larval skin ionocyte decreases as the ion-transport requirements are increasingly fulfilled by the gill ionocytes (Ayson et al., 1994; Hiroi et al., 1998, 1999; Varsamos et al., 2002; Kwan et al., 2019a). Recently, the ion-transporting capacity of larval skin ionocytes has been shown to be comparable to that of their adult counterpart, the gill ionocytes (Dahlke et al., 2020). Yet despite their differences in spatial localization, both skin and gill ionocytes rely on basolateral NKA to generate an electrochemical gradient necessary for maintaining osmotic and acid-base homeostasis. As a result, the immunostaining and quantification of NKA-rich ionocytes on the larva's epithelial surface can serve as a useful proxy for the ion-transporting capacity and underlying energetic demand.

The few studies that have explored the effects of OA on larval fish ionocytes found no significant differences in skin density (Dahlke et al., 2017), NKA expression, or NKA activity (Dahlke et al., 2020). Nonetheless, the increased otolith size and neurobehavioral alterations observed during exposure to elevated pCO$_2$ indicate that both larval and adult fishes maintain blood pH homeostasis by excreting H$^+$ and accumulating HCO$_3^-$ (reviewed in Tresguerres and Hamilton, 2017). This putative upregulation in acid-base homeostasis during OA exposure could entail increased energy consumption, which in turn could impair larval development and growth (Pimentel et al., 2014; Dahlke et al., 2017, 2020).

Basal energy consumption is commonly assessed through measurements of resting oxygen (O$_2$) consumption rate (rOCR) and somatic size (e.g. total length). Previous studies on the effects of OA on fish larvae reported diverse and variable results, with rOCR and body size increasing, decreasing, or remaining unchanged (Munday et al., 2009, 2016; Baumann et al., 2012; Miller et al., 2012; Bignami et al., 2013; Pimentel et al., 2014, 2015; Flynn et al., 2015; Rossi et al., 2015; Murray et al., 2016; Dahlke et al., 2017). As proposed in some of those studies, the variation in responses may be due to differences in pCO$_2$/pH exposure levels, duration, or unidentified species-specific physiological mechanisms that determined their differential vulnerability to OA. In addition, some studies have suggested the possibility of transgenerational acclimation (Miller et al., 2012; Munday, 2014; Murray et al., 2014; Cattano et al., 2016; Stiasny et al., 2018), whereby the duration and magnitude of the parental exposure to OA could positively affect their offspring's responses.

Aquaculture facilities can be an invaluable partner to research and fisheries management institutions, particularly through their ability to supply fish of ecological, commercial, or recreational importance for experiments. Broodstock may reside in recirculating aquarium systems (RAS) — aquaria with limited water exchange and controlled water parameters that prevent the growth of wild water-borne pathogens. Broodstock respiration typically results in elevated pCO$_2$ within the RAS at levels comparable to, and in many cases, greatly exceeding OA projections (reviewed in Ellis et al., 2016). However, due to the difficulty of reliably attaining wild-caught larvae and the challenges involved in spawning and raising larvae, aquaculture facilities are often the sole provider of larval fish for experimental research.

The Hubbs-SeaWorld Research Institute (HSWRI) in Carlsbad (California, USA) is the primary hatchery contractor for California's Ocean Resources Enhancement and Hatchery Program (OREHP) administered by the California Department of Fish and Wildlife. In an effort to replenish natural populations, HSWRI has been breeding and rearing white seabass (*Atractoscion nobilis*) within RAS for release into the Southern California Bight since 1986 (Vojkovich and Crooke, 2001; Hervas et al., 2010). Broodstock and early life stages are maintained in RAS for environmental control and biosecurity before being moved into flow through systems and then acclimation cages prior to release as juveniles (Drawbridge et al., 2021). HSWRI is also a long-term collaborator with the Scripps Institution of Oceanography (SIO) at the University of California, San Diego, and this partnership has contributed to novel insights supporting early observations of the impacts of elevated pCO$_2$ on fish larvae (Checkley et al., 2009). Two studies demonstrated significantly larger otoliths in larval white seabass pre-flexion larvae after exposure to 2500 µatm pCO$_2$ (Checkley et al., 2009; Shen et al., 2016). However, exposure to elevated pCO$_2$ and the ensuing enlarged utricular otoliths did not significantly impact the larva's vestibular function (Shen et al., 2016). The intention of this study is to expand upon these morphological and behavioral observations through an exploration of other aspects of larval white seabass physiology.

In this study, we exposed larval white seabass to control pCO$_2$ (560 ± 32 µatm) and elevated pCO$_2$ reflective of projected OA conditions (1971 ± 55 µatm) during the first five days post-fertilization (dpf). We hypothesized that exposure to OA conditions would induce an upregulation in acid-base machinery and corresponding increase in energy consumption. We proposed these physiological changes would be evident in the analysis of the skin ionocytes, relative NKA abundance, rOCR, and total length. A retroactive analysis of HSWRI RAS seawater chemistry records offered insights into broodstock conditions, and provided critical parental life history context to further understand our findings.

2. Materials and methods

Animal care and experimental procedures were approved by Institutional Animal Care and Use Committee at the University of California, San Diego under protocol S12161.

2.1. White seabass broodstock RAS conditions and egg collection

HSWRI routinely monitors and records broodstock RAS water conditions, including temperature every 15 min (RCK Controls; CA, USA), salinity and total alkalinity every week (Pinpoint®; American Marine, CT, USA), and HACH digital titrator (HACH, CO, USA), and O$_2$ and pH twice per day (HACH40d multimeter with LDO101 and PHC101 probes). Soda ash (Na$_2$CO$_3$) is added to RAS seawater as needed to maintain stable pH level as commonly performed by aquaculture facilities utilizing RAS. Seawater pCO$_2$ was calculated with CO2SYS using the recorded temperature, salinity, pH, and total alkalinity data. The accuracy of HSWRI's pH measurements was validated using the purified m-cresol purple method on discrete seawater samples as described below.

Larvae were spawned from adult white seabass (12 males and 12 females; >61 cm and >9.1 kg at the time of capture) that were captured in the wild between 2009 and 2012 and kept within RAS at HSWRI. Spawning at HSWRI is induced through photothermal manipulation by increasing 'daytime' duration from 10 to 14 h, and by raising seawater temperature from 14 °C to 18 °C to mimic the warmer spawning season. Fertilization occurs within the RAS and viable eggs float to the surface and are gently collected with a mesh at the outflow. In our study, eggs were collected on three separate occasions (June 15, June 29, and July 28, 2016) for three replicate experiments (EXP 1–3). For EXP 1, 2, and 3, the pH of the broodstock RAS at the time of egg collection was 7.39, 7.39, and 7.53, respectively. Fertilized white seabass eggs were transported to SIO within 12 h post-fertilization for inspection and initiation of experiments.

2.2. Experimental pCO_2 conditions

White seabass eggs were observed using a light microscope; undamaged, fertilized eggs were transferred into 5-L water-jacketed (18 °C) glass vessels (400 eggs/vessel) and larvae were reared until 5 dpf. The vessels contained filtered seawater continuously bubbled with certified air-CO_2 gas mixture resulting in average pCO_2 of 560 ± 32 µatm and pH of 7.92 ± 0.02 (control), and pCO_2 of 1971 ± 55 µatm and pH of 7.42 ± 0.03 (OA-exposed) (Supp. Table 1). The experiment was repeated three times, with each experiment having three vessels per treatment. High mortality was detected in one control and one OA-exposed vessel within EXP 3 for unknown reasons, and these two vessels were excluded from analysis.

At the end of the 5-day exposure, subsets of larvae were selected for microrespirometry or euthanized with tricaine methanesulfonate (0.5 g l^{-1}) and processed for immunohistochemistry or Western blotting. In EXP 1 and EXP 2, total length was measured immediately after euthanasia under a dissection microscope. In EXP 3, 2–4 dpf larvae were additionally sampled for total length measurements and immunohistochemistry.

At the end of each experiment, 250-mL seawater samples were collected from each vessel and poisoned with 100 µL of mercuric chloride for inorganic carbon chemistry measurements. A_T and dissolved inorganic carbon chemistry (DIC) were measured by the Dickson laboratory (SIO) using open-cell potentiometric titration and coulometry, respectively. The software CO_2Calc (Robbins et al., 2010) was used to estimate pH and pCO_2 from the measured A_T and DIC.

2.3. Immunohistochemistry

Larvae were fixed in 3% paraformaldehyde, 0.35% glutaraldehyde, 0.1 M cacodylate buffer (catalog number: 15949; Electron Microscopy Sciences, Hatfield, PA, USA) for 4 h at room temperature, transferred to 50% ethanol overnight, and stored in 70% ethanol. Whole-mount immunostaining was performed using the Vectastain® Universal HRP R.T.U. kit (Vector Laboratories, Inc., Burlingame, CA, USA) following a previously described protocol (Kwan et al., 2019b, a), and the α5 mouse monoclonal anti-NKA antibody (1.5 µg/mL) (Lebovitz et al., 1989) (Developmental Studies Hybridoma Bank; Iowa University). This antibody is routinely used for detecting NKA in fish (Melzner et al., 2009; Yang et al., 2013; Tang et al., 2014; Kwan et al., 2019a, 2020).

Immunostained larvae were imaged on a Leica DMR compound microscope (Leica Microsystems, Inc., Buffalo Grove, IL, USA) attached to a Canon Rebel T3i SLR camera and processed as previously described in detail (Kwan et al., 2019b). Briefly, the images were focal-stacked using Helicon Focus software (HeliconSoft, Kharkov, Ukraine) and stitched using Adobe Photoshop CS6 (Adobe Systems, San Jose, USA). Ionocytes were identified by intense NKA-immunostaining. Relative ionocyte area (RIA) was calculated as the number of cutaneous ionocytes multiplied by their average area, and divided by the larva's surface area (Kwan et al., 2019a, 2019b). Readers are referred to Kwan et al., 2019b for further methodological details. Measurements were made using the freehand tool from FIJI (Schindelin et al., 2012) and a Wacom Intuos tablet (Saitama, Japan).

2.4. Western blotting

Larvae were flash frozen in liquid N_2 and stored at -80 °C. Frozen larvae pooled from each vessel were pulverized in liquid N_2 by mortar and pestle, mixed in ice-cold homogenization buffer (250 mmol l^{-1} sucrose, 1 mmol l^{-1} EDTA, 30 mmol l^{-1} Tris, 10 mmol l^{-1} BHH, 1 mmol l^{-1} PMSF, 1 mmol l^{-1} DTT, pH 7.5), and centrifuged at 500g for 10 min at 4 °C to remove debris. The supernatant was saved ("crude homogenate"), and its total protein concentration was determined by Bradford Protein Assay. An additional sample that was not part of the experiments was designated as the standard and loaded into every gel to normalize results across immunoblots. Western blotting was performed as previously described (Kwan et al., 2019a, 2020), with 5 µg of total protein from each sample or standard loaded into a separate lane of the gels. The bands were imaged using the ChemiDoc™ MP system (Bio-Rad Laboratories, Inc., Hercules, CA, USA). The NKA antibody recognized a single band at the expected ~100 kDa (Supp. Fig. 2). Relative NKA abundance in each lane was quantified using Image Lab™ (Bio-Rad Laboratories, Inc.) and normalized relative to the standard.

2.5. Resting oxygen consumption rate

Larval resting O_2 consumption rate (rOCR) was measured using a Unisense MicroRespiration System and SensorTrace Rate software (Unisense A/S, Aarhus, Denmark). Ten larvae were removed from each vessel, and duplicate groups of five larvae were placed into two 4-mL glass microrespiration chambers containing seawater from the respective vessel. The seawater in the microrespirometry chamber was maintained at 18 °C by immersion into a water bath, and stirred at 600 rpm using a glass-embedded micromagnet. OCR measurements of groups of larvae are common given their small size (Cattano et al., 2016; Peck and Moyano, 2016).

After a 10 min acclimation period, O_2 concentration in the chamber was measured every second for 50 min. Larvae behavior was observed for 1 min every 15 min. Background microbial respiration rate was measured in chambers containing seawater only. The slope of the linear regression of O_2 concentration over time was taken as the rOCR for each group of five larvae. Duplicate measurements for each vessel were averaged and background microbial respiration was subtracted. The rOCR of an individual larva was estimated by dividing the group's rOCR by five. Statistical analyses were performed on these individual-based rOCR (µL O_2 ind^{-1} h^{-1}) estimates.

2.6. Data analysis

Statistical analyses were performed in GraphPad Prism (version 7.0a). Normality was assessed with the Shapiro-Wilks test. An alpha level of 0.05 was used for significance in all statistical tests. Linear regression was used to assess changes in RIA as a function of pCO_2 for larvae between 2 and 5 dpf. RIA, relative NKA abundance, rOCR, and total length were analyzed using two-tailed t-test. All experimental mean $\pm$ SEM, sample size, and statistical values are reported in Supp. Table 2.

3. Results

In EXP 1 and 2, we measured the total length of freshly-sacrificed 5 dpf larvae, and found that it was not significantly affected by OA exposure ($p = 0.6473$; Fig. 1A; Supp. Table 3). In EXP 3, we collected and fixed larvae between 2 and 5 dpf to investigate potential effects on
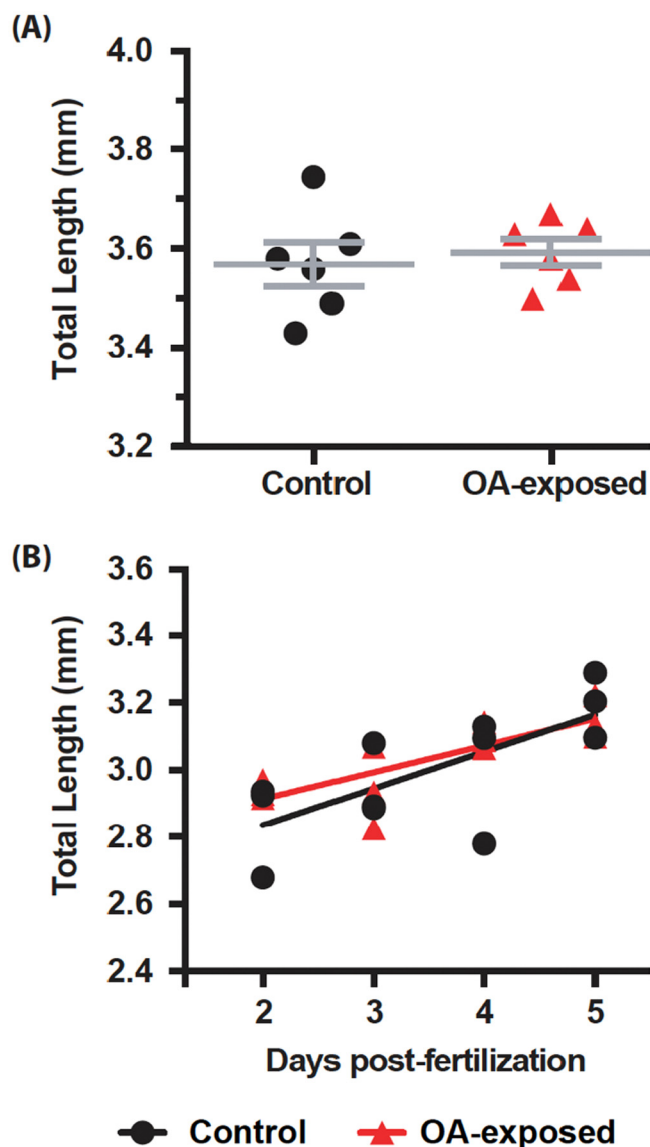
Fig. 1. Total length of experimental larval white seabass. Control (black, circle) and OA-exposed (red, triangle) larvae's (A) total length at 5 days post-fertilization ($t(10) = 0.4717$; $p = 0.6473$), and (B) over the 2 to 5 days post-fertilization ($F(1,20) = 0.6512$; $p = 0.4292$) were not significantly different. Data are presented as means ± S.E.M. (For interpretation of the references to color in this figure legend, the reader is referred to the web version of this article.)

growth rate. Similarly, OA exposure did not affect the larval white seabass' growth rate ($p = 0.4470$; Fig. 1B; Supp. Table 4).

Immunostaining of 5 dpf larvae revealed the cutaneous NKA-rich ionocytes were concentrated on the anterior end of both control and OA-exposed larvae (Supp. Fig. 4). OA-exposed larvae had a significantly higher number of ionocytes than control larvae ($p = 0.0410$; Fig. 2A; Supp. Table 5). Since the total larva surface area was virtually identical between treatments ($p > 0.9999$; Supp. Table 5), OA-exposed larvae had a significantly higher ionocyte density compared to control larvae ($p = 0.0008$; Fig. 2B; Supp. Table 5). However, ionocytes of OA-exposed larvae tended to be smaller than those of control larvae ($p = 0.0840$; Fig. 2C; Supp. Table 5). As a result, there were no differences in RIA between the control and OA-exposed larvae at 5 dpf ($p = 0.6129$; Fig. 2D; Supp. Table 5) indicative of similar total cutaneous ion-transporting capacities. This result was in alignment with the Western blot analysis showing a lack of significant difference in NKA abundance between OA-exposed and control larvae ($p = 0.2156$; Fig. 2E;

Supp. Fig. 2; Supp. Table 6). Similarly, the rate at which larval RIA decreased over the 2 to 5 dpf developmental period (Fig. 3) was not affected by OA exposure ($p = 0.6855$; Fig. 2F; Supp. Table 4).

Throughout microrespiration trials from EXP 1 and 2, larvae from both treatments remained largely inactive during experiments, occasionally engaging in swimming bursts to re-orient themselves. We found oxygen declined linearly as a result of larval respiration, but there were no significant differences in rOCR between OA-exposed and control larvae ($p = 0.928$; Fig. 4; Supp. Table 7).

The lack of any major physiological differences between control larvae and those exposed to elevated pCO_2 led us to conduct a retrospective analysis of the broodstock RAS seawater chemistry. Records indicated that the parents of the larval white seabass used in our study were exposed to an average of ~1200 µatm pCO_2 (pH ~7.6) at least 3.5 years prior to our experiment (Fig. 5A, B). The average total alkalinity, dissolved O_2 (DO), temperature, and salinity was 2289 ± 23 µmol kg^{-1} SW^{-1}, 9.10 ± 0.05 mg/L, 15.9 ± 2.3 °C, and 33.65 ± 0.03 ppt, respectively (Supp. Fig. 3). Furthermore, on the days the eggs were collected for our experiments, the pH of the outflowing water was 7.39 (~2073 ± 42 µatm), 7.36 (~2236 ± 45 µatm), and 7.53 (~1470 ± 15 µatm). Therefore, the RAS's pCO_2 levels are not only comparable to predicted OA-levels for the year 2300, but also analogous to our larval white seabass' experimental conditions.

4. Discussion

We hypothesized that exposure to elevated pCO_2 would increase the demand for ion-transport to maintain acid-base homeostasis by white seabass larvae, which would be reflected in higher RIA, NKA abundance, and rOCR. Contrary to our hypothesis, none of these variables were significantly different between control and OA-exposed larvae. Additionally, we did not detect differences in the growth parameters analyzed. Furthermore, our total length measurements were consistent with two previous larval white seabass OA studies (Checkley et al., 2009; Shen et al., 2016), thereby ruling out developmental differences. Altogether, our results indicate that white seabass larvae were able to cope with the elevated pCO_2 levels without significant ion-regulatory adjustments or any major additional energetic cost. Alternatively, the acid-base machinery and energetics of larval white seabass might have been affected in ways that were not measured in our experiment. Additionally, it remains unclear whether the chronic exposure to elevated pCO_2 within the broodstock tank could have had an effect on the larva's physiology, for example, through natural selection or transgenerational acclimation.

NKA is abundantly expressed in larval skin ionocytes, which allows for the identification and quantification of these ion-transporting cells using whole larva immunohistochemistry. Because NKA is the main driving force for ion-transport in marine fish, RIA and NKA abundance serve as proxies for ion-transporting capacity and its underlying energy demand. Traditionally, the ion-transporting capacity of fish larvae was estimated based on skin ionocyte density in a specific area of the fish (Ayson et al., 1994; Hiroi et al., 1998, 1999; Varsamos et al., 2002). In our experiment, skin ionocyte density in OA-exposed larvae was higher than in control larvae; however, ion-transporting capacity also depends on ionocyte size. To address this issue, we estimated RIA by measuring both ionocyte number and size as well as the surface area of the entire immunostained larvae. In doing so, RIA is a more accurate proxy for ion-transporting capacity than ionocyte density (Kwan et al., 2019a, 2019b). Interestingly, OA-exposed larvae had smaller average ionocyte size than control larvae. Although the difference in ionocyte size was not statistically significant, it resulted in OA-exposed and control larvae having similar RIA. Since these ionocytes have irregular shapes, we could not use simple math to calculate ionocyte volume. Instead, we used Western blotting to quantify total NKA protein within whole larvae as another proxy for ion-transporting capacity. This approach revealed lower total NKA abundance in OA-exposed larvae compared to
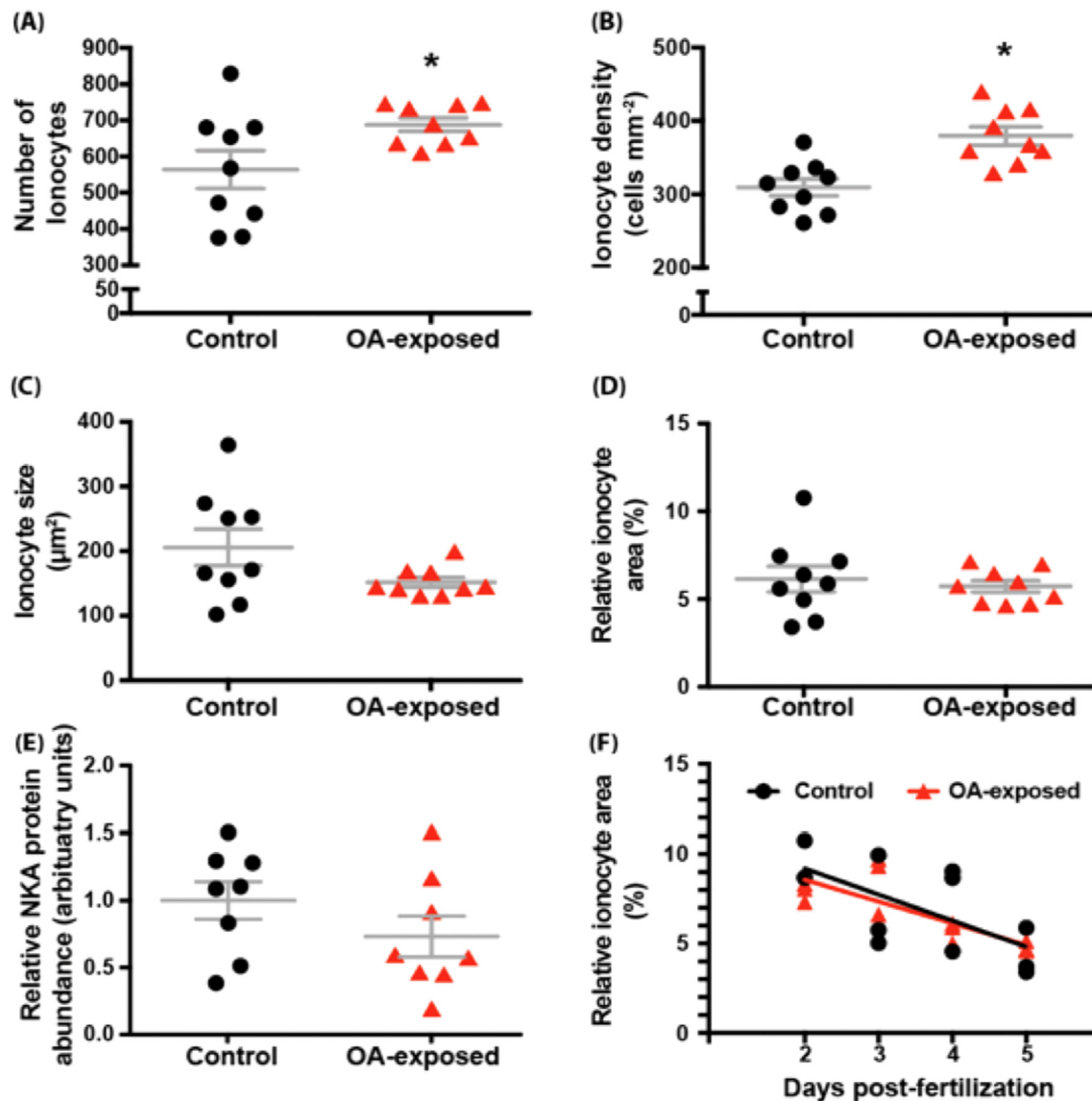
Fig. 2. Physiological responses of white seabass larvae exposed to control or OA conditions. The (A) number of ionocytes (t(16) = 2.223; p = 0.0410), (B) ionocyte density (t(16) = 4.106; p = 0.0008), (C) ionocyte size (t(16) = 1.843; p = 0.0840), (D) relative ionocyte area (t(16) = 0.5161; p = 0.6129), and (E) relative Na^+/K^+-ATPase abundance (t(14) = 1.297; p = 0.2156) of 5 days post-fertilization larvae exposed to control (black, circle) or OA (red, triangle) conditions. (F) The relative ionocyte area of larval white seabass over 2 to 5 days post-fertilization ((1,20) = 0.1689; p = 0.6855). Asterisks indicate significance at an alpha level of 0.05. Data are presented as means ± S.E.M. (For interpretation of the references to color in this figure legend, the reader is referred to the web version of this article.)

control larvae, but the difference was not statistically significant. Taken together, our results suggest that the ion-transporting capacities of OA-exposed and control larvae are similar, and that the observed differences in some of the parameters were due to inherent variability of the larvae and techniques.

Estimation of ion-transport capacity by immunodetecting NKA via immunohistochemistry and Western blotting is a powerful approach because it considers both the number and size of ionocytes in relation to larval size, as well as total NKA protein abundance. Since NKA is the most ATP-demanding step of ion-transport, NKA abundance serves as a proxy for energy utilization. However, the quantification of NKA abundance has various limitations that must be considered. In addition to H^+ excretion, the marine fish's NKA-rich ionocyte is also used for NaCl excretion to maintain nominal blood osmolarity, and presumably also NH_4^+ excretion and Ca^{2+} homeostasis (reviewed in Evans et al., 2005; Glover et al., 2013). Therefore, a putative increase in NKA abundance to upregulate H^+ excretion may not be detectable given the relatively high baseline levels from existing multi-functional physiological roles of the NKA-rich ionocyte. Furthermore, larval fishes grow at a very fast rate (Finn and Kapoor, 2008), and their rapidly metabolizing tissue determine rOCRs that are 50–80% higher than that of juveniles and adults (Post and Lee, 1996). As a result, the proportionally higher CO_2 production in larval fish coupled with their high reliance on ammonia-producing amino-acid catabolism (Finn et al., 2002) could entail an intrinsically high capacity for acid-base regulation that is sufficient to cope with the effects of OA without any major adjustments in NKA abundance or rOCR. Alternatively, the putative upregulation of H^+ excretion could have been achieved by increasing the abundance of other ion-transporting proteins such as Na^+/H^+ exchangers, Na^+/HCO_3^- cotransporters, and carbonic anhydrases that were not measured in our experiment.

The significant increase in protein biosynthesis or turnover rate should have been reflected in the rOCR measurements. For example, sea urchin and oyster larvae exposed to comparable pCO_2 levels
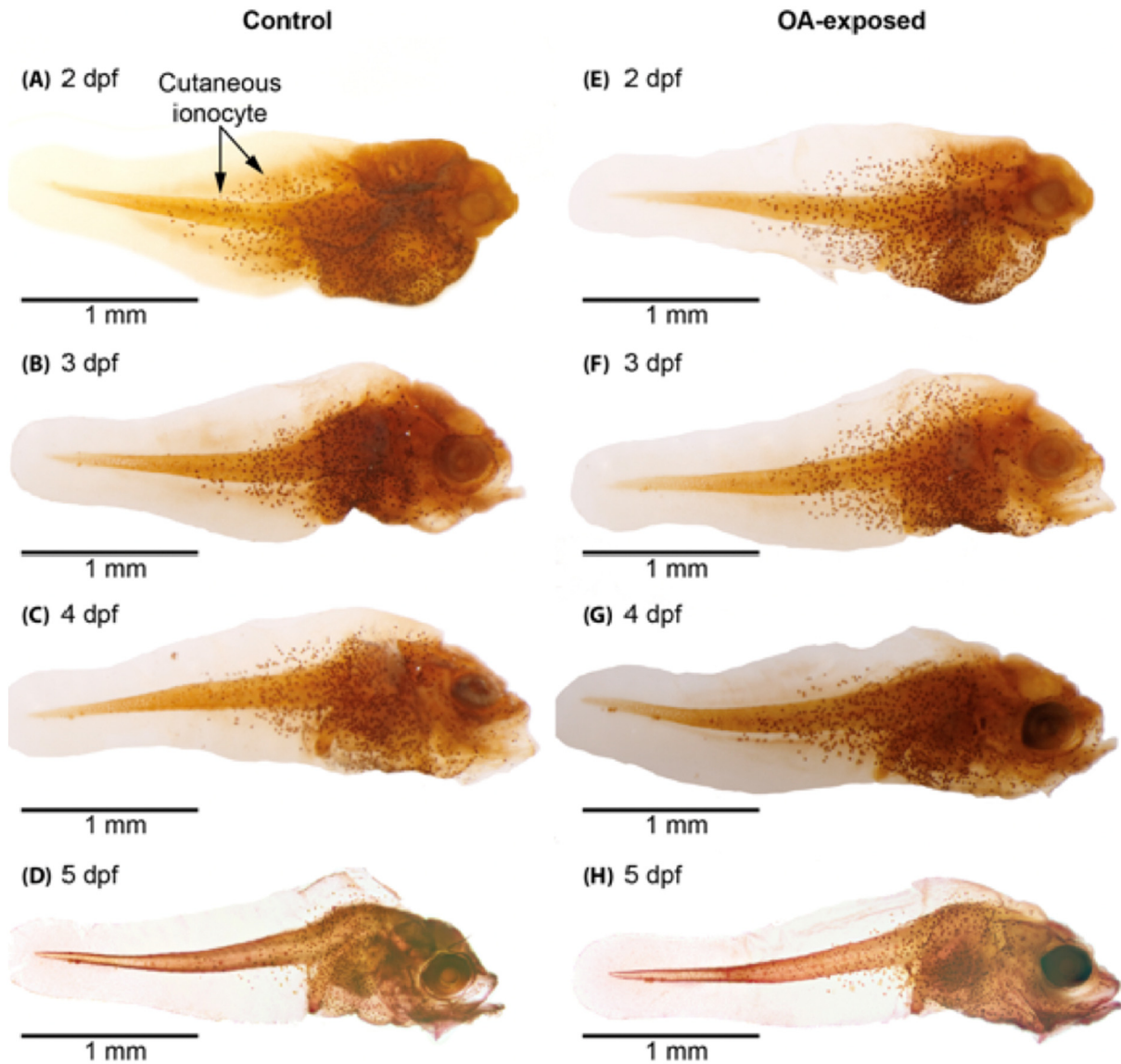
Fig. 3. Cutaneous ionocytes in white seabass larvae exposed to control or OA conditions. Representative images showing Na$^+$/K$^+$-ATPase immunostained cutaneous ionocytes in larvae. (A–D) control treatment; (E–H) OA-exposed treatment; dpf = days post-fertilization.

demonstrated both increased rOCR and protein turnover rates (Pan et al., 2015; Frieder et al., 2018). Alternatively, while we did not find evidence of increased protein biosynthesis, OA may have affected metabolic energy allocation. Since 5 dpf white seabass larvae still completely rely on their yolk sacs as their energy source (Moser et al., 1983), the allocation of energy towards protein biosynthesis would reduce the amount of energy available for other processes. Further studies examining protein biosynthesis are necessary to better understand the energetic responses of larval fishes to OA, which could be especially important in the presence of other stressors that impose additional energetic demand.

The retroactive analysis of HSWRI broodstock RAS conditions revealed an average pCO_2 of ~1,200 µatm during the 3.5 years prior to our experiments, and occasionally approached ~3000 µatm. As a consequence, the broodstock fish were chronically acclimated to elevated pCO_2 levels comparable to OA conditions predicted for the next century (Caldeira and Wickett, 2003, 2005; Goodwin et al., 2018; Bindoff et al., 2019). This raises the question of whether transgenerational acclimation influenced the larval white seabass

physiology within our study, and possibly contributing to the lack of significant differences between OA-exposed and control larvae. There is growing evidence indicating parental exposure to a given stressor may enhance offspring performance (reviewed in Donelson et al., 2018). Some possibilities include the maternal transmission of more efficient mitochondria [as proposed for Three-Spine Stickleback (*Gasterosteus aculeatus*) under thermal stress (Shama et al., 2014)] and of enhanced non-bicarbonate buffering capacity [suggested for Atlantic Cod (*Gadus morhua*) embryos (Dahlke et al., 2020)], and epigenetic modulation [as proposed for Spiny Damselfish (*Acanthochromis polyacanthus*) exposed to OA (Schunter et al., 2018)]. Interestingly, white seabass spawning, fertilization, and early embryo development also occur within the HSWRI RAS, and thus gametes and embryos are exposed to elevated pCO_2 during these crucial life stages. This suggests the possibilities of natural selection and developmental plasticity resulting in OA-resilient gametes, embryos, and larvae. Interestingly, if these effects indeed existed, the release of juveniles through OREHP (Vojkovich and Crooke, 2001; California Department of Fish and Game, 2002;
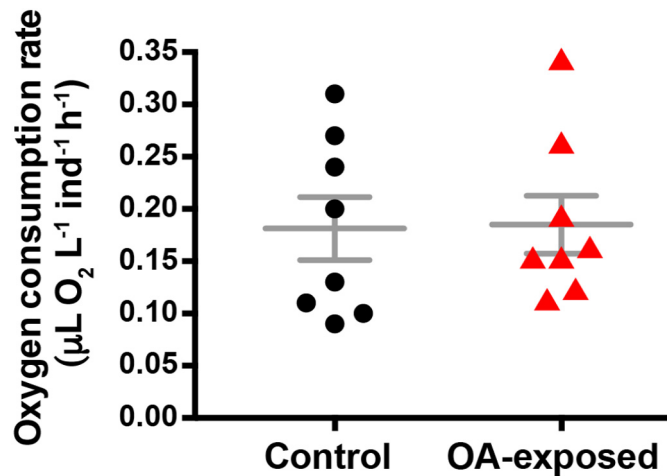
Fig. 4. Oxygen consumption rates of white seabass larvae. The oxygen consumption rate of white seabass larvae (in groups of 5) from EXP 1 were measured over a 50-minute period and shown as a function of time. No significant differences in oxygen consumption rate were detected between the larvae reared in control (black, circle) and those reared in OA-exposed (red, triangle) treatment ($t(14) = 0.0918$; $p = 0.928$). Data are presented as means ± S.E.M. (For interpretation of the references to color in this figure legend, the reader is referred to the web version of this article.)

Hervas et al., 2010) into the local ecosystem could be an example of an assisted evolution strategy similar to that proposed for coral reef resiliency (Van Oppen et al., 2015).

However, studying parental effects, developmental plasticity, and transgenerational mechanisms require a stringent experimental design (Donelson et al., 2018). Since our study was not designed to answer

these questions, it cannot discern whether the broodstock's chronic exposure to elevated pCO_2 had any effect on larval fitness. Nevertheless, the results presented here present a useful blueprint for future experiments, which, in addition to white seabass larvae from parental broodstock chronically acclimated to elevated pCO_2, must include larvae from broodstock acclimated to past- or present-day CO_2 levels (the "environmental" and "ambient" controls discussed in Donelson et al. (2018)). These types of studies will not be trivial due to the challenges associated with maintaining broodstock fish at different CO_2 levels during extended periods of time, achieving spawning, and rearing larvae. Performing these studies is further complicated by the relatively short duration of research funding schemes, student programs, and postdoctoral researcher contracts. With this in mind, it will remain crucial to continue to foster partnerships between academia and aquaculture facilities, which will allow to tackle essential questions that require extended experimentation periods such as transgenerational acclimation.

In conclusion, the lack of differences in RIA, NKA abundance, rOCR, and length obtained in the current study indicates that White Seabass larvae are able to cope with OA without major alterations in ion-transporting capacity, energy consumption, or growth when exposed to elevated pCO_2 (~2000 µatm) projected for the next century. However, in-depth analyses provided hints for potential novel effects such as changes in ionocyte size, and helped identify the need for more detailed studies about the basic physiology of marine fish larvae, their energy allocation in response to OA and multi-stressors, and the potential for transgenerational acclimation through parental effects, developmental plasticity, and natural selection. This highlights the difficulty of ascribing potential effects of OA on marine organisms based on acute laboratory studies. Finally, we would like to emphasize the importance of collaborations with aquaculture facilities, such as HSWRI, to continue advancing our understanding on the impacts of OA on fish.
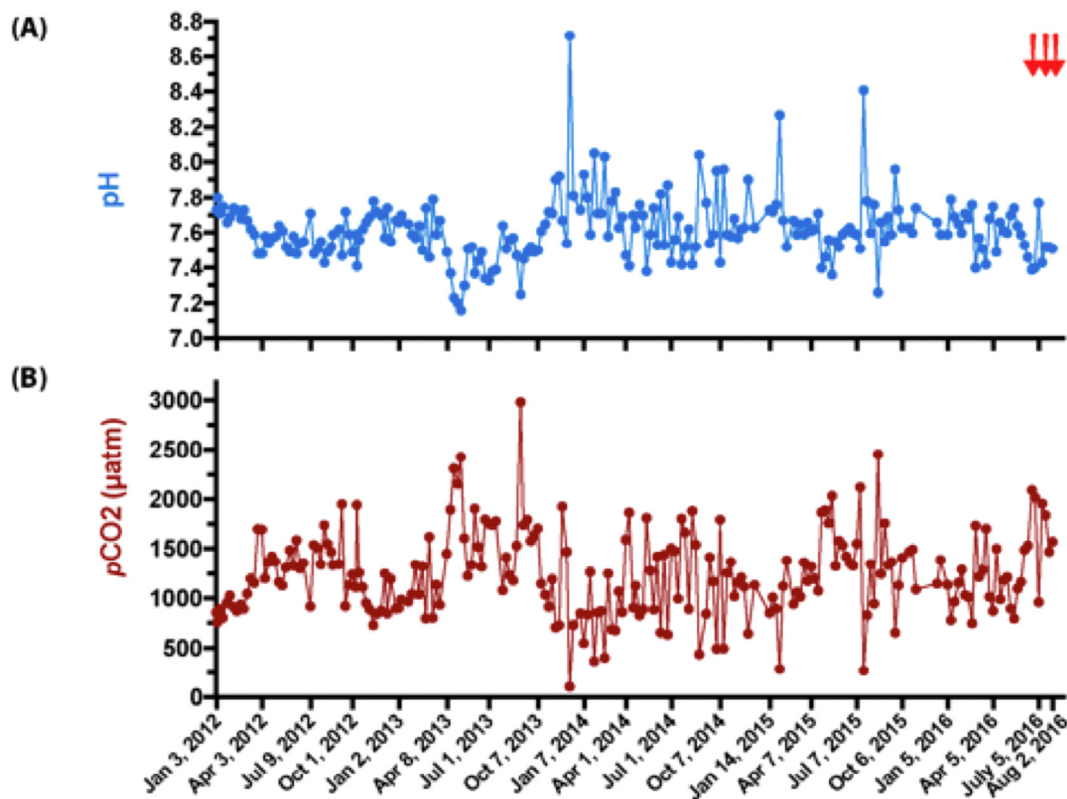
Fig. 5. Water chemistry of the white seabass broodstock tank in the 3.5 years previous to larval collection. (A) pH and (B) pCO_2. Red arrows on the top right indicate the date of egg collections. (For interpretation of the references to color in this figure legend, the reader is referred to the web version of this article.)

CRediT authorship contribution statement

S.G.S., G.T.K, M.T., and D.M.C. designed research; S.G.S. and G.T.K. performed research; S.G.S., G.T.K., and M.T. analyzed results and wrote the manuscript. M.D. provided historical data on white seabass broodstock holding conditions. D.M.C and M.D. provided guidance and reviewed draft manuscripts. All authors gave final approval for publication.

Declaration of competing interest

No competing interests declared.

Acknowledgements

Data availability

All data are available in our supplemental materials.

Appendix A. Supplementary data

Supplementary data to this article can be found online at https://doi.org/10.1016/j.scitotenv.2021.148285.

References

Ayson, F.G., Kaneko, T., Hasegawa, S., Hirano, T., 1994. Development of mitochondrion-rich cells in the yolk-sac membrane of embryos and larvae of tilapia, *Oreochromis mossambicus*, in fresh water and seawater. J. Exp. Zool. 270, 129–135. https://doi.org/10.1002/jez.1402700202.

Baumann, H., Talmage, S.C., Gobler, C.J., 2012. Reduced early life growth and survival in a fish in direct response to increased carbon dioxide. Nat. Clim. Chang. 2, 38–41. https://doi.org/10.1038/nclimate1291.

Beaugrand, G., Brander, K.M., Lindley, J.A., et al., 2003. Plankton effect on cod recruitment. Nature 426, 661–664.

Bignami, S., Sponaugle, S., Cowen, R.K., 2013. Response to ocean acidification in larvae of a large tropical marine fish, *Rachycentron canadum*. Glob. Chang. Biol. 19, 996–1006. https://doi.org/10.1111/gcb.12133.

Bindoff, N.L., Cheung, W.W.L., Kairo, J.G., et al., 2019. Changing ocean, marine ecosystems, and dependent communities. IPCC Spec Rep Ocean Cryosph a Chang Clim, pp. 447–588.

Caldeira, K., Wickett, M.E., 2003. Oceanography: anthropogenic carbon and ocean pH. Nature 425, 365. https://doi.org/10.1038/425365a.

Caldeira, K., Wickett, M.E., 2005. Ocean model predictions of chemistry changes from carbon dioxide emissions to the atmosphere and ocean. J. Geophys. Res. C Oceans 110. https://doi.org/10.1029/2004jc002671 (12 pp.-12 pp.).

Cattano, C., Giomi, F., Milazzo, M., 2016. Effects of ocean acidification on embryonic respiration and development of a temperate wrasse living along a natural CO2 gradient. Conserv. Physiol. 4, 1–10. https://doi.org/10.1093/conphys/cov073.

CDFG, 2002. White Seabass Fishery Management Plan (WSFMP). Los Alamitos.

Checkley, D.M., Dickson, A.G., Takahashi, M., et al., 2009. Elevated CO2 enhances otolith growth in young fish. Science 324, 1683. https://doi.org/10.1126/science.1169806.

Dahlke, F.T., Leo, E., Mark, F.C., et al., 2017. Effects of ocean acidification increase embryonic sensitivity to thermal extremes in Atlantic cod, *Gadus morhua*. Glob. Chang. Biol. 23, 1499–1510. https://doi.org/10.1111/gcb.13527.

Dahlke, F.T., Lucassen, M., Bickmeyer, U., et al., 2020. Fish embryo vulnerability to combined acidification and warming coincides with a low capacity for homeostatic regulation. J. Exp. Biol. 223, jeb212589. https://doi.org/10.1242/jeb.212589.

Donelson, J.M., Salinas, S., Munday, P.L., Shama, L.N.S., 2018. Transgenerational plasticity and climate change experiments: where do we go from here? Glob. Chang. Biol. 24, 13–34. https://doi.org/10.1111/gcb.13903.

Drawbridge, M., Shane, M., Silbernagel, C., 2021. The status of white seabass, *Atractoscion nobilis* as a commercially ready species for marine US aquaculture. J. World Aquacult. Soc., 1–15 https://doi.org/10.1111/jwas.12772.

Ellis, R.P., Urbina, M.A., Wilson, R.W., 2016. Lessons from two high CO2 worlds - future oceans and intensive aquaculture. Glob. Chang. Biol. 2100, 1–8. https://doi.org/10.1111/gcb.13515.

Esbaugh, A.J., 2017. Physiological implications of ocean acidification for marine fish: emerging patterns and new insights. J. Comp. Physiol. B. 0, 0. https://doi.org/10.1007/s00360-017-1105-6.

Evans, D.H., Piermarini, P.M., Choe, K.P., 2005. The multifunctional fish gill: dominant site of gas exchange, osmoregulation, acid-base regulation, and excretion of nitrogenous waste. Physiol. Rev. 85, 97–177. https://doi.org/10.1152/physrev.00050.2003.

Finn, R.N., Kapoor, B., 2008. Fish Larval Physiology.

Finn, R.N., Rønnestad, I., Van der Meeren, T., Fyhn, H.J., 2002. Fuel and metabolic scaling during the early life stages of Atlantic cod *Gadus morhua*. Mar. Ecol. Prog. Ser. 243, 217–234. https://doi.org/10.3354/meps243217.

Flynn, E.E., Bjelde, B.E., Miller, N.A., Todgham, A.E., 2015. Ocean acidification exerts negative effects during warming conditions in a developing Antarctic fish. Conserv. Physiol. 3, 1–16. https://doi.org/10.1093/conphys/cov033.

Frieder, C.A., Applebaum, S.L., Pan, T.C.F., Manahan, D.T., 2018. Shifting balance of protein synthesis and degradation sets a threshold for larval growth under environmental stress. Biol. Bull. 234, 45–57. https://doi.org/10.1086/696830.

Frommel, A.Y., Maneja, R., Lowe, D., et al., 2011. Severe tissue damage in Atlantic cod larvae under increasing ocean acidification. Nat. Clim. Chang. 2, 42–46. https://doi.org/10.1038/nclimate1324.

Glover, C.N., Bucking, C., Wood, C.M., 2013. The skin of fish as a transport epithelium: a review. J. Compr. Physiol. B Biochem. Syst. Environ. Physiol. 183, 877–891. https://doi.org/10.1007/s00360-013-0761-4.

Goodwin, P., Brown, S., Haigh, I.D., et al., 2018. Adjusting mitigation pathways to stabilize climate at 1.5°C and 2.0°C rise in global temperatures to year 2300. Earths Future 6, 601–615. https://doi.org/10.1002/2017EF000732.

Hervas, S., Lorenzen, K., Shane, M.A., Drawbridge, M.A., 2010. Quantitative assessment of a white seabass (*Atractoscion nobilis*) stock enhancement program in California: post-release dispersal, growth and survival. Fish. Res. 105, 237–243. https://doi.org/10.1016/j.fishres.2010.06.001.

Heuer, R.M., Grosell, M., 2014. Physiological impacts of elevated carbon dioxide and ocean acidification on fish. AJ. Regul. Integr. Compr. Physiol. 307, R1061–R1084. https://doi.org/10.1152/ajpregu.00064.2014.

Hiroi, J., Kaneko, T., Seikai, T., Tanaka, M., 1998. Developmental sequence of chloride cells in the body skin and gills of Japanese Flounder (*Paralichthys olivaceus*) larvae. Zool. Sci. 15, 455–460. https://doi.org/10.2108/0289-0003(1998)15[455:DSOCCI]2.0.CO;2.

Hiroi, J., Kaneko, T., Tanaka, M., 1999. In vivo sequential changes in chloride cell morphology in the yolk-sac membrane of Mozambique tilapia (*Oreochromis mossambicus*) embryos and larvae during seawater adaptation. J. Exp. Biol. 202, 3485–3495.

Hjort, J., 1926. Fluctuations in the year classes of important food fishes. J. Cons. Int. Explor. Mer 1, 5–38.

Houde, E.D., 2009. Recruitment variability. In: Fish Reproductive Biology: Implications for Assessment and Management. Wiley-Blackwell, West Sussex, pp. 91–171.

Ishimatsu, A., Hayashi, M., Kikkawa, T., 2008. Fishes in high-CO2, acidified oceans. Mar. Ecol. Prog. Ser. 373, 295–302. https://doi.org/10.3354/meps07823.

Kwan, G.T., Wexler, J.B., Wegner, N.C., Tresguerres, M., 2019a. Ontogenetic changes in cutaneous and branchial ionocytes and morphology in yellowfin tuna (*Thunnus albacares*) larvae. J. Comp. Physiol. B Biochem. Syst. Environ. Physiol. 189, 81–95. https://doi.org/10.1007/s00360-018-1187-9.

Kwan, G.T., Finnerty, S.H., Wegner, N.C., Tresguerres, M., 2019b. Quantification of cutaneous ionocytes in small aquatic organisms. Bio-protocol 9, e3227. https://doi.org/10.21769/BioProtoc.3227.

Kwan, G.T., Smith, T.R., Tresguerres, M., 2020. Immunological characterization of two types of ionocytes in the inner ear epithelium of Pacific Chub Mackerel (*Scomber japonicus*). J. Comp. Physiol. B. 190, 419–431. https://doi.org/10.1007/s00360-020-01276-3.

Lebovitz, R.M., Takeyasu, K., Fambrough, D.M., 1989. Molecular characterization and expression of the (Na++K+)-ATPase alpha-subunit in *Drosophila melanogaster*. EMBO J. 8, 193–202.

Meehl GA, Stocker TF, Collins WD, et al (2007) 2007: Global climate projections. In: Climate Change 2007: Contribution of Working Group I to the Fourth Assessment Report of the Intergovernmental Panel on Climate Change. Cambridge University Press, Cambridge, UK, pp. 747–846

Melzner, F., Gutowska, M.A., Langenbuch, M., et al., 2009. Physiological basis for high CO2 tolerance in marine ectothermic animals: pre-adaptation through lifestyle and ontogeny? Biogeosci. Discuss. 6, 4693–4738. https://doi.org/10.5194/bgd-6-4693-2009.

Miller, G.M., Watson, S.A., Donelson, J.M., et al., 2012. Parental environment mediates impacts of increased carbon dioxide on a coral reef fish. Nat. Clim. Chang. 2, 858–861. https://doi.org/10.1038/nclimate1599.

Moser, G.H., Ambrose, D.A., Busby, M.S., et al., 1983. Description of early stages of white seabass, *Atractoscion nobilis*, with notes on distribution. CalCOFI Rep. 24, 182–193.

Munday, P.L., 2014. Transgenerational acclimation of fishes to climate change and ocean acidification. F1000Prime Rep. 6, 1–7. https://doi.org/10.12703/P6-99.

Munday, P.L., Donelson, J.M., Dixson, D.L., Endo, G.G.K., 2009. Effects of ocean acidification on the early life history of a tropical marine fish. Proc. R. Soc. B Biol. Sci. 276, 3275–3283. https://doi.org/10.1098/rspb.2009.0784.

Munday, P.L., Watson, S.-A., Parsons, D.M., et al., 2016. Effects of elevated CO2 on early life history development of the yellowtail kingfish, *Seriola lalandi*, a large pelagic fish. ICES J. Mar. Sci. 73, 641–649. https://doi.org/10.1093/icesjms/fsv210.

Murray, C., Malvezzi, A., Gobler, C., Baumann, H., 2014. Offspring sensitivity to ocean acidification changes seasonally in a coastal marine fish. Mar. Ecol. Prog. Ser. 504, 1–11. https://doi.org/10.3354/meps10791.

Murray, C.S., Fuiman, L.A., Baumann, H., 2016. Consequences of elevated CO2 exposure across multiple life stages in a coastal forage fish. ICES J. Mar. Sci., fsw179 https://doi.org/10.1093/icesjms/fsw179.

Pan, T.C.F., Applebaum, S.L., Manahan, D.T., 2015. Experimental ocean acidification alters the allocation of metabolic energy. Proc. Natl. Acad. Sci. U. S. A. 112, 4696–4701. https://doi.org/10.1073/pnas.1416967112.

Peck, M.A., Moyano, M., 2016. Measuring respiration rates in marine fish larvae: challenges and advances. J. Fish Biol. 88, 173–205. https://doi.org/10.1111/jfb.12810.

Pimentel, M.S., Faleiro, F., Dionisio, G., et al., 2014. Defective skeletogenesis and oversized otoliths in fish early stages in a changing ocean. J. Exp. Biol. 217, 2062–2070. https://doi.org/10.1242/jeb.092635.

Pimentel, M.S., Faleiro, F., Diniz, M., et al., 2015. Oxidative stress and digestive enzyme activity of flatfish larvae in a changing ocean. PLoS One 10, e0134082. https://doi.org/10.1371/journal.pone.0134082.

Post, J., Lee, J., 1996. Metabolic ontogeny of teleost fishes. Can. J. Fish. Aquat. Sci. 53, 910–923. https://doi.org/10.1139/f95-278.

Robbins L, Hansen M, Kleypas J, Meylan S (2010) CO2Calc - A User-friendly Seawater Carbon Calculator for Windows, Max OS X, and iOS (iPhone). 1–17.

Rossi, T., Nagelkerken, I., Simpson, S.D., et al., 2015. Ocean acidification boosts larval fish development but reduces the window of opportunity for successful settlement. Proc. R. Soc. B Biol. Sci. 282, 20151954. https://doi.org/10.1098/rspb.2015.1954.

Schindelin, J., Arganda-Carreras, I., Frise, E., et al., 2012. Fiji: an open-source platform for biological-image analysis. Nat. Methods 9, 676–682. https://doi.org/10.1038/nmeth.2019.

Schunter, C., Welch, M.J., Nilsson, G.E., et al., 2018. An interplay between plasticity and parental phenotype determines impacts of ocean acidification on a reef fish. Nat. Ecol. Evol. 2, 334–342. https://doi.org/10.1038/s41559-017-0428-8.

Shama, L.N.S., Strobel, A., Mark, F.C., Wegner, K.M., 2014. Transgenerational plasticity in marine sticklebacks: maternal effects mediate impacts of a warming ocean. Funct. Ecol. 28, 1482–1493. https://doi.org/10.1111/1365-2435.12280.

Shen, S.G., Chen, F., Schoppik, D.E., Checkley, D.M., 2016. Otolith size and the vestibulo-ocular reflex of larvae of white seabass Atractoscion nobilis at high pCO2. Mar. Ecol. Prog. Ser. 553, 173–182. https://doi.org/10.3354/meps11791.

Stiasny, M.H., Mittermayer, F.H., Göttler, G., et al., 2018. Effects of parental acclimation and energy limitation in response to high CO2 exposure in Atlantic cod. Sci. Rep., 1–8 https://doi.org/10.1038/s41598-018-26711-y.

Tang, C.H., Leu, M.Y., Yang, W.K., Tsai, S.C., 2014. Exploration of the mechanisms of protein quality control and osmoregulation in gills of Chromis viridis in response to reduced salinity. Fish Physiol. Biochem. 40, 1533–1546. https://doi.org/10.1007/s10695-014-9946-3.

Tresguerres, M., Hamilton, T.J., 2017. Acid-base physiology, neurobiology and behaviour in relation to CO2 -induced ocean acidification. J. Exp. Biol. 220, 2136–2148. https://doi.org/10.1242/jeb.144113.

Van Oppen, M.J.H., Oliver, J.K., Putnam, H.M., Gates, R.D., 2015. Building coral reef resilience through assisted evolution. Proc. Natl. Acad. Sci. U. S. A. 112, 2307–2313. https://doi.org/10.1073/pnas.1422301112.

Varsamos, S., Diaz, J., Charmantier, G., et al., 2002. Location and morphology of chloride cells during the post-embryonic development of the European sea bass, Dicentrarchus labrax. Anat. Embryol. (Berl.) 205, 203–213. https://doi.org/10.1007/s00429-002-0231-3.

Vojkovich, M., Crooke, S., 2001. White seabass. California's Living Resources: A Status Report. Cal Fish Game, Sacramento, pp. 206–208.

Yang, W., Kang, C., Chang, C., et al., 2013. Expression Profiles of Branchial FXYD Proteins in the Brackish Medaka Oryzias dancena: A Potential Saltwater Fish Model for Studies of Osmoregulation. https://doi.org/10.1371/journal.pone.0055470.

Appendices
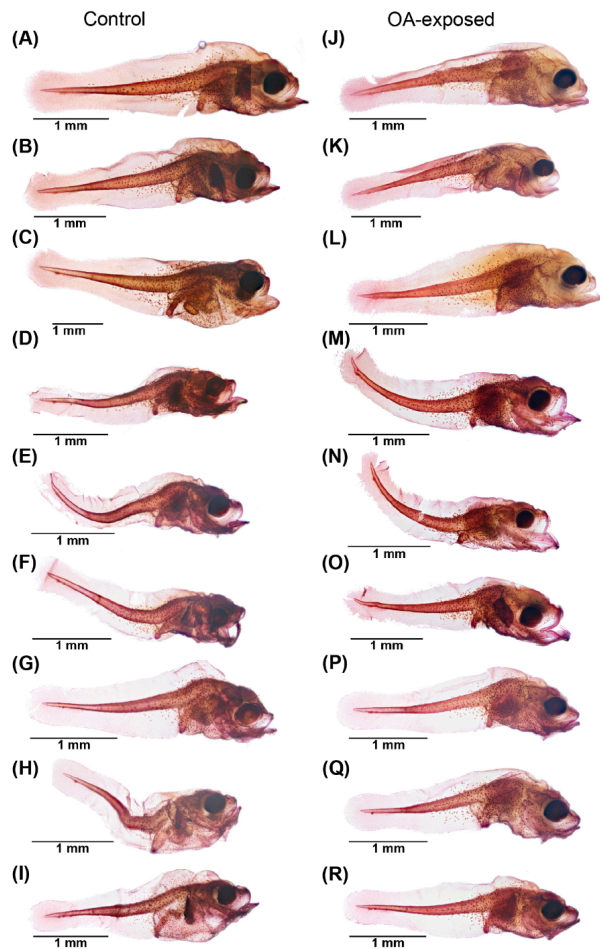
Supp. Fig. 1. Images of white seabass larvae with immunostained cells labeled with a Na$^+$/K$^+$-ATPase antibody. Images show the distribution of cutaneous immunopositive cells for control (n = 9) (A-I) and OA-exposed (n = 9) (J-R) larvae of all experiments. The relative ionocyte area dataset is available in Supplemental Table 3 and 4.

7
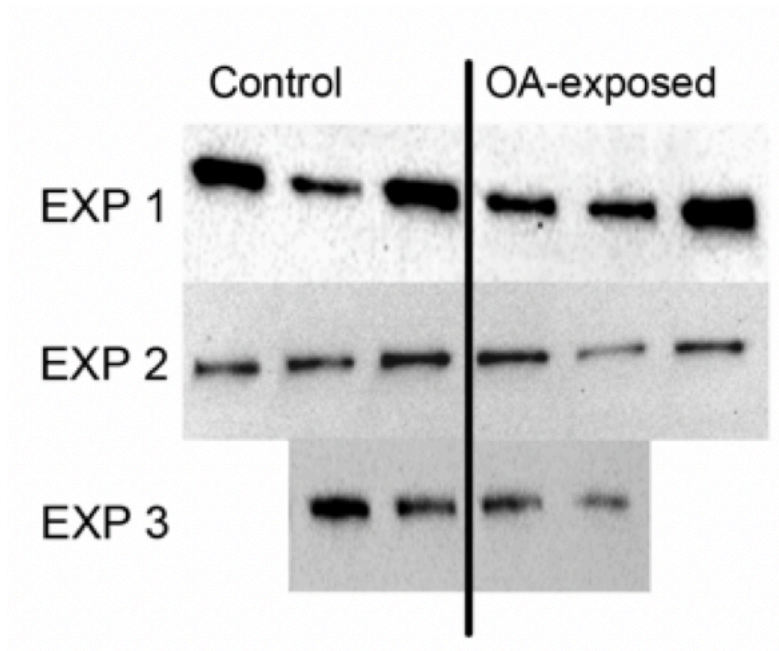
Supp. Fig. 2. Western blots analysis of Na$^+$/K$^+$-ATPase (NKA) abundance in white seabass larvae exposed to control or OA conditions. Relative NKA abundance was quantified using western blot. Each lane of larval white seabass crude homogenate yielded a single band at ~100 kDa. The dataset is available in Supplemental Table 5.

12
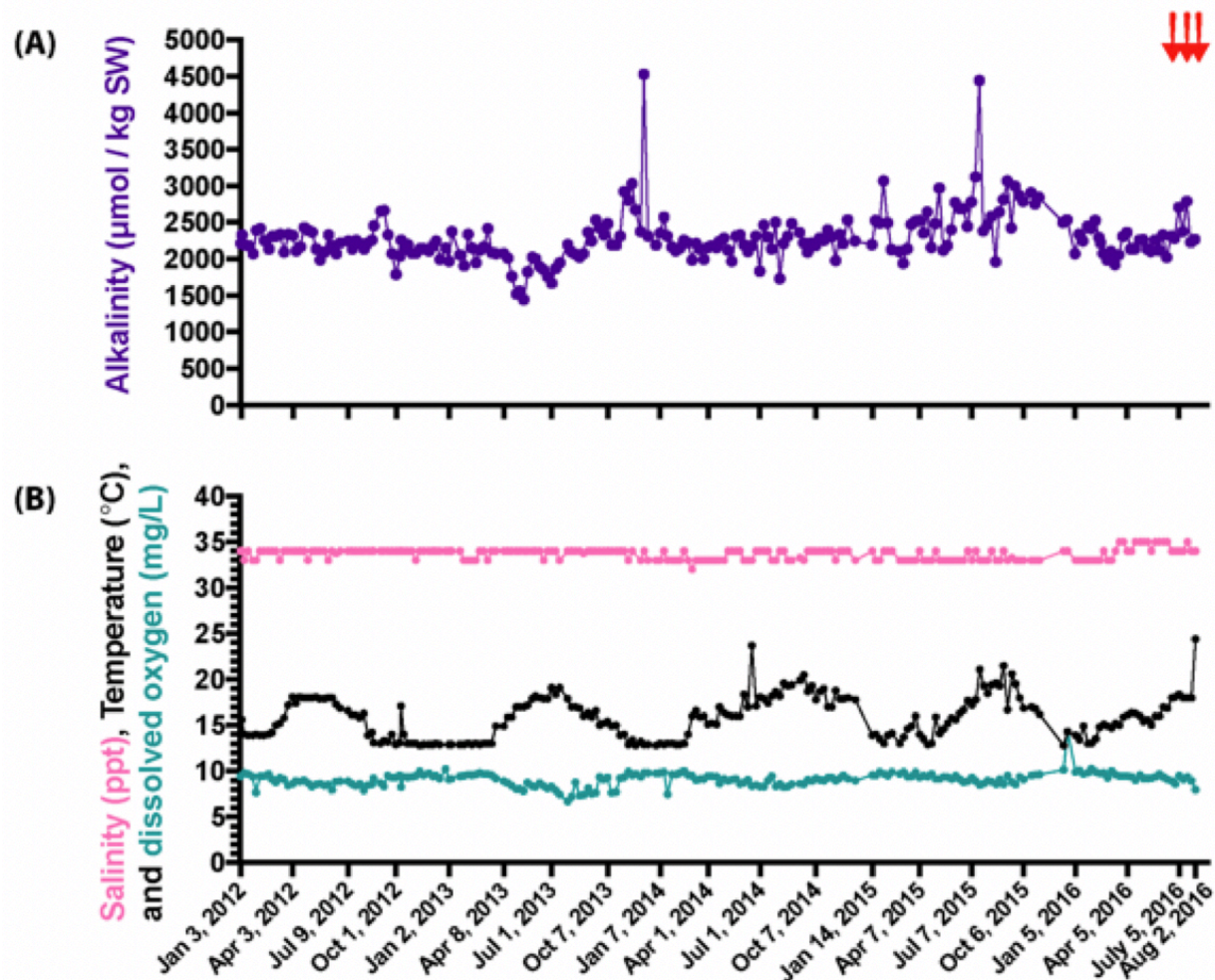
Supp. Fig. 3. Water chemistry of tank where broodstock fishes were held. Adult white

seabass were collected between 2009 – 2012, and housed within a recirculating aquaculture

system at the Hubbs-SeaWorld Research Institute. The (A) alkalinity, (B) salinity, temperature,

and dissolved oxygen are reported from January 2012 to August 2016. The red arrows on the

top right indicate the date of egg collections. The pH and pCO_2 values are shown in Figure 5.

18

19

20

21

22

23 **Supplemental Table 1. Seawater carbonate chemistry measurements of larval incubation**

24 **vessels.** Values are measured salinity (Sal), temperature (Temp), total alkalinity (A_T) and

25 dissolved inorganic carbon (DIC) for each of the control and OA-exposed vessels for all

26 experiments. Average (Avg) pH and pCO_2 ± standard error of the mean (SEM) are also

27 provided per treatment for each EXP. Partial pressure of CO_2 (pCO_2) and pH were estimated

28 using the software CO2Calc.

EXP	Vessel	Sal	Temp (°C)	A_T (μmol kg^{-1})	DIC (μmol kg^{-1})	pH	Avg pH	pCO_2 (μatm)	Avg pCO_2 (μatm)
1	1	33.64	18.0	2262.0	2102.3	7.89	7.92 ± 0.01	601	565.33 ± 18.02
	2	33.62	18.0	2270.2	2095.7	7.93		552	
	3	33.65	18.0	2269.9	2092.5	7.93		543	
1	4	33.61	18.1	2262.5	2271.6	7.39	7.39 ± 0.00	2097	2112 ± 16.52
	5	33.64	18.0	2259.4	2268.9	7.39		2094	
	6	33.64	18.0	2264.3	2276.6	7.38		2145	
2	7	33.61	18.0	2269.2	2061.7	7.99	7.95 ± 0.02	454	508.67 ± 33.32
	8	33.61	18.0	2263.5	2094.9	7.91		569	
	9	33.64	18.0	2268.0	2078.3	7.96		503	
2	10	33.60	18.0	2263.1	2253.0	7.45	7.46 ± 0.00	1799	1789.33 ± 6.49
	11	33.61	18.1	2269.5	2258.2	7.46		1792	
	12	33.62	18.0	2263.5	2251.9	7.46		1777	
3	13	33.63	18.0	2257.9	2070.3	7.96	7.88 ± 0.07	506	630 ± 101.25
	14	33.62	18.1	2247.7	2123.3	7.80		754	
3	15	33.63	18.0	2262.6	2266.3	7.41	7.41 ± 0.00	2005	2033 ± 22.86
	16	33.62	18.1	2244.5	2252.2	7.40		2061	

29

30

31

32

33

34

35

Supplemental Table 2. Summary of larval white seabass response to ~2,000 µatm of

pCO_2. Values are presented as mean ± standard error of the mean (SEM). Statistical

significance denoted at p < 0.05 (alpha = 0.95).

	Control		OA		Statistics
	Mean ± SEM	N	Mean ± SEM	N	
Experimental Vessel (pH)	7.92 ± 0.02	8	7.42 ± 0.03	8	**t(14) = 21.19; p < 0.0001**
Experimental Vessel (µatm of pCO_2)	560 ± 32	8	1971 ± 55	8	**t(14) = 22.16; p < 0.0001**
Total Length [Fresh] (mm)	3.57 ± 0.04	6	3.59 ± 0.03	6	t(10) = 0.4717; p = 0.6473
Total Length over 2 - 5 dpf [Fixed] (mm dpf^{-1})	0.129 ± 0.083 vs.	12	0.060 ± 0.019	12	F(1,20) = 0.6512; p = 0.4292
Ionocyte Number (cells per mm^2)	564.6 ± 52.43	9	688.2 ± 18.59	9	**t(16) = 2.223; p = 0.0410**
Larval Surface Area (mm^2)	1.833 ± 0.04	9	1.833 ± 0.17	9	t(16) = 0; p > 0.9999
Ionocyte Density (cells µm^{-2})	309.60 ± 11.62	9	379.70 ± 12.51	9	**t(16) = 4.106; p = 0.0008**
Ionocyte Size (µm^2)	205.94 ± 28.34	9	152.09 ± 7.44	9	t(16) = 1.843; p = 0.0840
Relative Ionocyte Area (%)	6.14 ± 0.74	9	5.73 ± 0.27	9	t(16) = 0.5161; p = 0.6129
Relative NKA Abundance	1.00 ± 0.14	8	0.73 ± 0.15	8	t(14) = 1.297; p = 0.2156
Relative Ionocyte Area over 2 - 5 dpf (% dpf^{-1})	-1.46 ± 0.51	12	-1.22 ± 0.30	12	F(1,20) = 0.1689; p = 0.6855
Resting Oxygen Consumption Rate (µL O$_2$ ind^{-1} h^{-1})	0.18 ± 0.03	8	0.19 ± 0.03	8	t(14) = 0.0918; p = 0.928

Supplemental Table 3. Total length of 5 days post-fertilization larvae. The total length of

49 freshly-sacrificed control and OA-exposed larval white seabass was sampled from EXP 1 and 2.

50

51

EXP	Vessel	dpf	Treat	Average Length (mm)
1	1	5	Low	3.74
1	2	5	Low	3.58
1	3	5	Low	3.61
1	1	5	High	3.58
1	2	5	High	3.63
1	3	5	High	3.67
2	1	5	Low	3.49
2	2	5	Low	3.56
2	3	5	Low	3.43
2	1	5	High	3.64
2	2	5	High	3.54
2	3	5	High	3.50

52

53

54

55

56

57

58

59

60

61

62

63

64

65

66

67 **Supplemental Table 4. Relative ionocyte area for 2 to 5 days post-fertilization larvae as**

68 **determined by whole-body immunohistochemistry.** In EXP 3, larval measurements were

69 made per dpf (2, 3, 4, and 5) and per treatment (control and OA-exposed). Unlike those

70 reported in Supplemental Table 3, the total length measurements reported here are made after

71 fixation and dehydration. The data on 5 days post-fertilization larvae are also presented in Fig.

72 2, and included in Supplemental Figure 1 and Supplemental Table 2. Immunohistochemistry

73 images are shown in Figure 3.

EXP	dpf	treatment	TL (mm)	RIA (%)
3	2	Low	2.9	8.6957
3	2	Low	2.7	10.7508
3	2	Low	2.9	8.6773
3	2	High	2.9	7.331
3	2	High	3.0	8.3506
3	2	High	2.9	8.0661
3	3	Low	2.9	5.0334
3	3	Low	3.1	9.9453
3	3	Low	2.9	5.7583
3	3	High	3.1	9.3398
3	3	High	2.9	9.7218
3	3	High	2.8	6.6251
3	4	Low	3.1	9.0471
3	4	Low	3.1	4.5578
3	4	Low	2.8	8.6746
3	4	High	3.1	5.0003
3	4	High	3.1	5.9174
3	4	High	3.1	6.1165
3	5	Low	3.1	3.4099
3	5	Low	3.3	3.7067
3	5	Low	3.2	5.8826
3	5	High	3.2	4.7101
3	5	High	3.1	4.6186
3	5	High	3.1	5.1401

74

75

76

77

78

79 **Supplemental Table 5. Ionocyte count, ionocyte size, ionocyte density, and relative**

80 **ionocyte area for 5 days post-fertilization larvae as determined by whole-body**

81 **immunohistochemistry.** Measurements were made for three 5 days post-fertilization larvae

82 from one control and OA-exposed vessel per experiment. Data are presented in Figure 2.

EXP	dpf	treatment	cell count	cell size (mm2)	Surface Area (mm2)	Density (cell / mm2)	RIA (%)
1	5	Low	680	0.000274	2.5	272	7.45
1	5	Low	654	0.00025102	2.3	283	7.14
1	5	Low	829	0.00036372	2.6	315	10.77
1	5	High	733	0.00016732	1.9	392	6.45
1	5	High	609	0.00019948	1.7	359	7.15
1	5	High	690	0.00014527	2.1	329	4.77
2	5	Low	472	0.00016583	1.4	336	5.59
2	5	Low	376	0.00017131	1.3	296	4.95
2	5	Low	379	0.00025267	1.5	261	6.38
2	5	High	748	0.00013037	1.7	440	5.74
2	5	High	746	0.00014428	1.8	416	5.98
2	5	High	743	0.00016898	1.8	413	6.98
3	5	Low	568	0.00010206	1.7	329	3.41
3	5	Low	443	0.00011714	1.4	323	3.71
3	5	Low	680	0.00015572	1.8	371	5.88
3	5	High	635	0.00014093	1.9	341	4.71
3	5	High	637	0.00013051	1.8	359	4.62
3	5	High	653	0.00014169	1.8	368	5.14

83

84

85

86

87

88

89

90

91

Supplemental Table 6. Relative NKA abundance from whole-body crude homogenates of larvae from western blots. A group of fish larva independent of the experiment was used as a reference standard to normalize results across gels. Images of the western blots are presented in Supplemental Figure 2.

EXP	dpf	Treat	Relative NKA Abundance
1	5	Low	1.280
1	5	Low	0.384
1	5	Low	1.296
1	5	High	0.592
1	5	High	0.576
1	5	High	1.504
2	5	Low	1.088
2	5	Low	1.104
2	5	Low	1.504
2	5	High	1.168
2	5	High	0.464
2	5	High	0.912
3	5	Low	0.832
3	5	Low	0.512
3	5	High	0.448
3	5	High	0.192

96

97

98

99

100

101

102

103

104 **Supplemental Table 7. Oxygen consumption rates of white seabass larvae.** Individual-

105 based O_2 consumption rates of control and OA-exposed larvae for all experiments. Data are

106 presented in Figure 4.

EXP	dpf	Treat	OCR ($\mu L\ O_2\ ind^{-1}\ h^{-1}$)
1	5	Low	0.24
1	5	Low	0.13
1	5	Low	0.20
1	5	High	0.16
1	5	High	0.19
1	5	High	0.15
2	5	Low	0.11
2	5	Low	0.09
2	5	Low	0.10
2	5	High	0.15
2	5	High	0.12
2	5	High	0.11
3	5	Low	0.31
3	5	Low	0.27
3	5	High	0.34
3	5	High	0.26

107

108